Published in final edited form as:
Angiogenesis. 2012 September ; 15(3): 469–480. doi:10.1007/s10456-012-9275-z.

Vascular adaptation to a dysfunctional endothelium as a consequence of *Shb* deficiency

Gustaf Christoffersson,
Department of Medical Cell Biology, Uppsala University, Box 571, Husargatan 3, 75123 Uppsala, Sweden

Guangxiang Zang,
Department of Medical Cell Biology, Uppsala University, Box 571, Husargatan 3, 75123 Uppsala, Sweden

Zhen W. Zhuang,
Department of Cardiovascular Medicine, Yale University, New Haven, CT, USA

Evelina Vågesjö,
Department of Medical Cell Biology, Uppsala University, Box 571, Husargatan 3, 75123 Uppsala, Sweden

Michael Simons,
Department of Cardiovascular Medicine, Yale University, New Haven, CT, USA

Mia Phillipson, and
Department of Medical Cell Biology, Uppsala University, Box 571, Husargatan 3, 75123 Uppsala, Sweden

Michael Welsh
Department of Medical Cell Biology, Uppsala University, Box 571, Husargatan 3, 75123 Uppsala, Sweden

Michael Welsh: Michael.welsh@mcb.uu.se

Abstract

Vascular endothelial growth factor (VEGF)-A regulates angiogenesis, vascular morphology and permeability by signaling through its receptor VEGFR-2. The *Shb* adapter protein has previously been found to relay certain VEGFR-2 dependent signals and consequently vascular physiology and structure was assessed in *Shb* knockout mice. X-ray computed tomography of vessels larger than 24 μm diameter (micro-CT) after contrast injection revealed an increased frequency of 48–96 μm arterioles in the hindlimb calf muscle in *Shb* knockout mice. Intravital microscopy of the cremaster muscle demonstrated a less regular vasculature with fewer branch points and increased

Correspondence to: Michael Welsh, Michael.welsh@mcb.uu.se.

Gustaf Christoffersson and Guangxiang Zang have equally contributed.

Electronic supplementary material The online version of this article (doi:10.1007/s10456-012-9275-z) contains supplementary material, which is available to authorized users.

Conflict of interest The authors declare no conflicts of interests.

vessel tortuosity, changes that led to an increased blood flow velocity. Reduced in vivo angiogenesis was observed in *Shb* knockout Matrigel™ plugs. Unlike the wild-type situation, VEGF-A did not provoke a dissociation of VE-cadherin from adherens junctions in *Shb* knockout venules. The reduced angiogenesis and altered properties of junctions had consequences for two patho-physiological responses to arterial occlusion: vascular permeability was reduced in the *Shb* knockout cremaster muscle after ligation of one supplying artery and heat-induced blood flow determined by Laser-Doppler measurements was decreased in the hindlimb after ligation of the femoral artery. Consequently, the *Shb* knockout mouse exhibited structural and functional (angiogenesis and vascular permeability) vascular abnormalities that have implications for understanding the function of VEGF-A under physiological conditions.

Keywords

VEGF; VE-cadherin; Adherens junctions and permeability; Angiogenesis; Src homology-2 protein B; Blood flow

Introduction

The vasculature has attracted considerable attention during the last few decades due to its importance for pathological processes such as cardiovascular disease, inflammation and cancer biology [1, 2]. Understanding normal vascular function is a prerequisite for addressing its role in pathology. Although a wealth of knowledge on the vasculature exists, there are still crucial gaps that need to be addressed. Of particular interest are the three following aspects of vascular function: angiogenesis, blood flow and vascular permeability. Vascular endothelial growth factor-A (VEGF-A) is the primary angiogenic factor operating through the stimulation of VEGFR-2 [3] and this factor causes endothelial cells to proliferate, migrate and release proteases that initiate an invasive reaction. These processes in concert generate nascent vascular sprouts with tips [4]. Other factors, such as angiopoietin-1 and -2, fibroblast growth factor-2 (FGF-2), epidermal growth factor, hepatocyte growth factor etc. also participate in angiogenesis and the maintenance of the microvasculature [5–7].

Blood flow is regulated by numerous factors such as adenosine, adrenaline, nitric oxide and others by constriction/dilatation of arterioles in response to demand [8, 9]. Arterial blood flow is clearly essential for vascular development [10, 11] and there is nothing at present that excludes the possibility that arterial morphogenesis and angiogenesis at the microvascular level are orchestrated in a synchronized manner since VEGF-A also potently stimulates arterial endothelial cells [12]. An example illustrating a potential interrelationship between arterial and microvascular angiogenesis is the fact that during inhibition of tumor angiogenesis, an increased vascular/capillary perfusion was commonly observed [13, 14]. Besides normalized structural features of the capillary bed, it is also conceivable that the arterial supply is stimulated to compensate for decreased capillary bed volume ensuing as a consequence of anti-angiogenic treatment. Therefore, the stimulated arteriolar supply could be a functional response to vasoregulatory factors through constricting/dilating effects on

arterioles and/or by altered arterial structural features as a consequence of morphogenesis in this vascular component.

Another aspect of vascular function is vascular permeability and VEGF-A as a factor that provokes a strong vascular permeability response [15]. The mechanisms behind this effect are not fully characterized, although certain data hint at VEGFR-2 dependent dissociation of adherens junctions as a possible mechanism [16]. The cell–cell interacting molecule VE-cadherin is the primary organizer of junction assembly/disassembly thus regulating permeability [17, 18]. Alternatively, permeability may result from transport through vesiculo-vacuolar organelles [19]. In addition, permeability may arise from gaps in endothelial junctions in response to inflammatory agents [20, 21].

The Src-homology 2 protein B (*Shb*) is an adapter protein operating downstream of VEGFR-2 [22]. An abnormal endothelial compartment was observed in *Shb* knockout mice that causes reduced tumor growth [23]. The endothelial ultrastructure and VE-cadherin and CD31 staining patterns were less distinct in knockout endothelial cells. These morphological aberrations correlated with reduced VEGF-stimulated vascular permeability and decreased angiogenesis. The results were taken to reflect altered VEGFR-2 signaling. However, the findings did not take the function of arterioles or venules into consideration, and consequently, to what extent the abnormal endothelial compartment affected other functional characteristics of the vasculature.

The present study was conducted in order to understand the role of *Shb* in normal vascular physiology by using the *Shb* mutant mouse. We were particularly intrigued by the possibility that changes in endothelial cells could by coordinated or compensatory mechanisms affect the function or structural features of other vascular components such as arterioles and venules. Consequently, the hindlimb and cremaster vasculatures were studied in this mutant mouse in attempts to relate a dysfunctional endothelium with these other vascular compartments. Endothelial dysfunction was noted with respect to both angiogenesis and integrity of junctions. We also observed vascular aberrations in the larger vessels that may reflect coordinated or compensatory responses to endothelial dysfunction.

Materials and methods

Animals

The *Shb* knockout mouse [24] was obtained on a FVBN/C57Bl6/129SvJ background. Mice between ages of 2–5 months were used for the current study. At regular intervals, +/+ and −/− mice were crossed with each other to generate +/−offspring and new +/+ and −/− founders established from such +/− parents to reduce genetic drifting with time. All animal experiments were approved by the local animal ethics committee at the Uppsala County Court.

Cremaster muscle preparation

The cremaster muscle of mice on heating pads and under 2 % isoflurane anesthesia (Abbott Scandinavia, Sweden) was exposed on a transparent viewing pedestal. The muscle vasculature was visualized in an intravital microscope and images recorded via a high-

sensitivity CCD-camera (Orca-R2, Hamamatsu, Japan) at high frame-rates using Volocity Acquisition 5.0 software (PerkinElmer, Waltham, MA, USA).

Intravital plasma flow measurements

A catheter (PE 10, inner diameter 0.28 mm, outer diameter 0.61 mm) was placed in the femoral artery to enable a close intra-arterial route to the cremaster muscle vasculature. Through this, repeated small (less than 10 μl) and rapid bolus injections of FITC (fluorescein isothiocyanate)-dextran (70 kDa, Sigma-Aldrich, St. Louis, MO, USA) were injected retrogradely while green fluorescence signal from blood vessels was recorded. The flow of the injected fluorescent dextran during the transition from arterioles, through capillaries to post-capillary venules was semi-automatically measured using Volocity Quantitation 5.0 (PerkinElmer).

Quantification of vascular branching and density in cremaster muscle

In vivo soybean agglutinin (SBA)-lectin-perfused cremaster muscle vasculature was imaged to cover a major part of the muscle. Images were tiled in Adobe Photoshop CS3 (Adobe, USA) and the compiled images imported into ImageJ. Branching was quantified by binarizing the images and by using the plugin AnalyzeSkeleton to evaluate the vascular tree. Total blood vessel density was quantified by measuring percent lectin positive area in the two-dimensional intravital images in ImageJ.

Whole-mount staining of cremaster muscle

Fluorescently conjugated CD31-antibody (clone 390/Alexa Fluor 555, eBioscience, San Diego, CA, USA/Invitrogen, Carlsbad, CA, USA) was injected intra-arterially at the end of experiments. The exposed cremaster muscle was excised, fixated in ice-cold methanol and further stained with antibodies against CD31 (BD Bioscience, Franklin Lakes, NJ, USA) and VE-cadherin (R&D Systems, Minneapolis, MN, USA) followed by Alexa Fluor 488 or 594 conjugated secondary antibodies (Invitrogen) to ensure complete staining of all vascular structures including those that could have escaped the intra-arterially injected CD31-antibody. Imaging was performed immediately after cremaster muscle excision and after CD31/VE-cadherin staining in a laser scanning confocal microscope.

In vivo vascular response to VEGF-A

Endothelial cell junctions were injected with conjugated CD31-antibody as above. Recombinant human VEGF-A (hrVEGF-A, R&D Systems) (1 ng) in 50 μl phosphate-buffered saline (PBS) was injected intra-arterially—leading to direct and efficient delivery to the left cremaster muscle. After 5 min, the cremaster was excised and processed as above. Quantification of VE-cadherin localization to adherens junctions was done as follows: grids were placed over VE-cadherin stained venules and the percentage cross points detected over non-stained venular area was counted manually and calculated in percent of total venular area. Values are for 3–5 independent observations.

Scanning electron microscopy (SEM)

Cremaster muscles were perfusion fixed with 2.5 % glutaraldehyde +1 % paraformaldehyde, dehydrated and cut with a razor. SEM was performed on gold covered (30 nm) surfaces. Open (loose or porous) adherens junctions were quantitated as follows: the length of junctions was measured on SEM images using a ruler and the relative fraction (in percent) corresponding to open junctions (loose or porous according to representative images in Fig. 4) was measured as well on the same junctions. Values are for 6–12 separate images.

Vascular permeability in response to ischemia

Ischemia was induced in cremaster muscles of mice by electrocauterization of one of the major intra-cremasteric arteries using finely tipped tweezers, disrupting the blood supply to approximately half of the muscle. Experiments were performed either at 1 or 24 h after occlusion of the artery. SBA-lectin (100 μg, Invitrogen) was injected via the femoral artery to stain perfused blood vessels. The cremaster muscle was then exposed for intravital observation, and 300 μg rhodamine-dextran (70 kDa, Sigma-Aldrich) was injected intra-arterially. The vascular leakage was imaged 10 min post-injection and the fluorescence intensity was measured using ImageJ (NIH, Bethesda, MD, USA).

In vivo Matrigel™ plug assay

hrVEGF-A (R&D Systems) and FGF-2 (R&D Systems) at final concentrations of 0.5 μg/ml in cool sterile PBS were mixed by pipetting with regular Matrigel™ (BD Bioscience). After anesthesia with 2 % isofluorane, 350 μl of growth factor containing Matrigel™ at 4 °C was injected subcutaneously into the abdominal region of 3 *Shb* −/− or *Shb* +/+ mice. On day 7 the animals were sacrificed, the Matrigel™ plugs were carefully removed including as little tissue surrounding the Matrigel™ plugs as possible, frozen in liquid nitrogen and stored at −70 °C prior to whole-mount CD31/VE-cadherin staining as described above.

Micro-CT imaging

Mice were heparinized with 100 IU undiluted heparin (1,000 USP U/ml) after receiving 0.02 ml/g body weight of 2.5 % 1 g/ml 2,2,2-tribromoethanol (Sigma-Aldrich) dissolved in 2-methyl-2-butanol (Avertin). Once sacrificed, descending thoracic aorta was cannulated with a 25-gauge blunt butterfly needle for aortic retrograde perfusion of PBS containing 4 mg/l papaverin and 1 g/l adenosine for 3 min, 2 % paraformaldehyde for 5 min, and PBS flush for 2 min, followed by 0.2 ml/10 g body weight home-made 20 % Bismuth in 5 % gelatin at 0.75 ml/min using an automatic, mechanical injector [25]. After completion of vascular perfusion, the mouse was covered with wet ice for over 30 min to polymerize the contrast agent. The hind-limbs were then dissected from the body and stored in 2 % paraformaldehyde overnight.

The hindlimb vasculature was imaged with a high-resolution micro-CT imaging system (GE eXplore Locus SP, GE Healthcare, Milwaukee, WI, USA) set to a 0.008-mm effective detector pixel size [25]. Micro-CT was operated at 60-kVp x-ray tube voltage, 100-mA tube current, 2,960-milli-second per frame, 1 × 1 detector binning model, 720 views, and 0.5°

increments per view. This acquisition resulted in a set of contiguous axial VFF-formatted images through each sample.

Image reconstruction and quantitative image analysis

With the use of Microview Software (GE Healthcare), the raw data was corrected and reconstructed with voxels of dimensions 16 μm × 16 μm × 16 μm to visualize the whole vascular tree. After the above reconstructed micro-CT data set was transferred to the Advanced Workstation (version 4.4; GE Healthcare), different post-processing techniques enabled us to extract the vasculature and re-batch this reconstructed imaging according to the re-orientated central line along the long axis of the major vessel using modified method [26] for quantitation. For quantitation, a volume of interest was reconstructed of the hindlimb calf muscle (200 slices). A semi-automated algorithm was used to extract detailed morphometric data on the diameter, area, numbers of vessels, and distribution of different sizes of vessels by using modified software (ImageJ; National Institutes of Health, Bethesda, MD, USA). Finally, the total area and volume could be summed up for each muscle. The data was expressed as vascular segment numbers, representing the total numbers of vessels of specified diameters, and counted in all reformatted cross-sections.

Hindlimb blood flow measurements after femoral artery occlusion

Mice were anesthetized (Isoflurane, 2 %, Abbott Scandinavia, Sweden) and the fur was removed from both legs (Veet, Recitt Benckiser, Valora Trade, Stockholm, Sweden). To induce hind limb ischemia the left femoral artery was separated from the femoral vein, ligated and cut above the superficial epigastric artery branch as previously described [27].

Tissue perfusion was measured non-invasively in the knee region of anesthetized mice 1, 3 and 7 days after artery ligation, using Laser Doppler flowmetry (PeriFlux 4001 Master, Perimed, Järfälla, Sweden) with 780 nm laser light applied directly onto the skin. Shifted backscattered light was collected via 0.5 mm fiber separated laser probes. Paw skin temperature was continuously recorded using an isolated thermistor transducer (MLT422/A) connected to a thermistor Pod (ML309) both AD Instruments, Oxford, United Kingdom.

Baseline tissue perfusion was recorded (30 min) in room temperature whereafter heat was applied to the entire limb for 30 min through tubing containing pre warmed water. Data was converted by PowerLab 4/3 and analyzed using LabChart 7 Pro software, both AD Instruments, Oxford, United Kingdom. Blood flow is expressed as delta perfusion units.

Statistical analysis

Means ± SEM are given for the number of observations described in each legend. Students' *t* tests were used to provide an assessment for chance differences between the groups compared.

Results

Increased density of intermediately sized arterioles in *Shb* knockout hindlimb calf muscle observed by micro-CT

To understand the vascular structure in *Shb* knockout mice, the hindlimb calf muscle arterial system was visualized by micro-CT (X-ray computed tomography of contrast injected vasculature) to determine whether any structural aberrations of the arterial tree could be detected. The impression of the volume rendered images was that of a denser arterial tree in the *Shb* knockout hindlimb vasculature (Fig. 1a). Quantitation of the calf muscle vascular density revealed a trend towards an increased vascular density in the *Shb* knockout of all size ranges (Fig. 1b). This trend became statistically significant when the vascular density of the 48–96 μm range was compared, corresponding to intermediately sized arterioles. These differences could reflect an adaptive structural response to the impaired microvasculature (see below) and have functional implications allowing a compensatory increase in blood flow.

Increased blood flow velocity and microvascular abnormalities of *Shb* knockout cremaster muscle

Due to its anatomical location and thinness, the cremaster muscle can be exteriorized allowing studies of the functional vasculature in a living animal using intravital microscopy. This muscle has under steady-state no ongoing angiogenesis. Arterial injection of a fluorescent dye visualized the cremaster vasculature. Fig. 2a showed primarily the arterial/arteriolar vasculature directly after close intra-arterial injection of FITC-dextran. The *Shb* knockout arterial vasculature displayed more irregularities and increased number of smaller/intermediately sized arterioles (exemplified by arrows in both genotypes). A similar pattern of vascular irregularities was also noted when the cremaster muscle was stained for CD31 by close intra-arterial injections of antibodies and subjected to confocal microscopy at a higher magnification primarily visualizing capillaries (Fig. 2b). The morphology was supplemented with functional analysis by measuring the passage time of the dye. Passage time was decreased, indicating elevated blood flow velocity over the local arteriolar/capillary network. In addition, the average distance from a larger artery (seen in top of panels) to a larger venule was increased in the knockout, corroborating the visual impression of less regularity and increased tortuosity (Fig. 2c). The capillary bed was also quantified but no significant difference in microvascular density was noted between the wild-type and knockout (Fig. 2c). However, when quantifying capillary branchpoints, a lower value was recorded in the *Shb* knockout (Fig. 2c), reinforcing the notion that absence of *Shb* indeed results in an abnormal microvasculature. Thus, the data suggest vascular abnormalities in the *Shb* knockout that have functional consequences.

Impaired Matrigel™ angiogenesis in *Shb* knockout mice

Whereas the characterization of the cremaster vasculature was performed on an organ not undergoing active angiogenesis, it was of interest to compare the results in Fig. 2 with those obtained in a situation exhibiting active angiogenesis. For the latter purpose, subcutaneous Matrigel™ angiogenesis was investigated (Fig. 3). We have previously reported reduced Matrigel™ angiogenesis and to substantiate those findings further we performed whole-

mount staining and confocal volume rendering of Matrigel™ plugs. The data revealed dramatically reduced angiogenesis in *Shb* knockout mice in response to VEGF-A plus FGF-2 (Fig. 3). Not only was the vascular density reduced (Fig. 3), but also the number of vessel tips and branch-points, indicating impaired angiogenesis in *Shb* knockout mice that provides a likely explanation for the vascular abnormalities observed in the cremaster muscle.

Morphology of venule adherens junctions

In addition to its pro-angiogenic role, VEGF-A is known to be a potent inducer of vascular permeability. Adherens junctions, key components participating in the regulation of this process, were characterized in small venules in the cremaster muscle by CD31 (Supplemental Fig. 1) or VE-cadherin staining of fixated muscle samples (Fig. 4a). Addition of VEGF-A to the cremaster vasculature caused rapid changes in the VE-cadherin staining pattern in wildtype venules (Fig. 4a). Whereas VE-cadherin co-localized with adherens junctions under non-stimulated conditions, VEGF-A caused its dissociation from these and allowed VE-cadherin to dissipate throughout the endothelial cells (Fig. 4a). This effect was quantitated (Fig. 4b) and found to be significantly different from that recorded in the unstimulated situation. In the *Shb* knockout, no distinct changes in response to VEGF-A were observed (Fig. 4a, b). The corresponding panels for CD31 staining are shown in Supplemental Fig. 1, revealing intact endothelial morphology in the VEGF-A stimulated wild-type situation. Ultrastructural corroboration of these data was obtained by scanning electron microscopy (SEM). In wild-type venules without stimulation, regular junctions were observed that mostly appeared closed (Fig. 4c, see arrow in non-stimulated wild-type). VEGF-A dissociated such junctions by unfolding them and causing them to form a flap that was partly loose and extending over the adjacent cell. In some instances, pores were detected (Fig. 4c, see arrow in VEGF-A stimulated wild-type). In *Shb* knockout venules that had not been exposed to VEGF-A, an irregular junctional morphology was observed that contained both closed and loose junctions (Fig. 4c, see arrow for example of loose junction with a flap that extended over the adjacent cell in non-stimulated *Shb* knockout). VEGF-A addition exerted no major effect on junction morphology with a large fraction of closed junctions (Fig. 4c, see arrow in VEGF-A stimulated *Shb* knockout) remaining. Quantitation of the junctions, categorizing them as either closed or open (“loose” or “porous” according to the morphological criteria visualized by the arrows in Fig. 4c) revealed that VEGF-A opened the junctions in the wild-type but not knockout venules (Fig. 4d). In summary, *Shb* knockout venular endothelium exhibited structural aberrations in the presence of VEGF-A that may have functional consequences.

Reduced vascular permeability in response to cremaster arterial ligation in *Shb* knockout mice

The relevance of the altered structural features of *Shb* knockout endothelium was assessed in relation to occlusion of one of the two major arteries supplying the cremaster muscle. Such a procedure will immediately reduce total cremaster blood flow followed by a reduction in local oxygenation. However, the cremaster muscle is rich on collaterals and therefore no part of the muscle was completely devoid of blood supply after the procedure (results not shown). Whereas no difference in vascular permeability between wild-type and *Shb*

knockout cremaster muscle was observed prior to ligation, the procedure provoked a response that 24 h later revealed reduced vascular permeability in the *Shb* knockout muscle distal to the site of ligation (Fig. 5). Consequently, the structural aberrations of *Shb* knockout adherens junctions will alter the physiological response to the ischemia that ensues as a consequence of arterial ligation.

Reduced hindlimb blood flow in response to increased temperature after femoral artery ligation in *Shb* knockout mice

Another model for vascular responses is femoral artery occlusion followed by blood flow determinations, commonly denoted as the “hindlimb ischemia” model. We subjected wild-type and *Shb* knockout mice to this experimental procedure and followed hindlimb blood flow just above the knee on day 1, day 3 and day 7 after surgery. The response in the healthy leg was also analyzed. The basal blood flow of the uninjured leg in the *Shb* knockout (52 ± 4 PFU) tended to be increased ($p = 0.03$) compared with the corresponding wild-type (41 ± 2 PFU) value whereas in the legs exposed to surgery no difference was noted (*Shb* knockout 38 ± 3 PFU and wild-type 36 ± 3 one day after surgery). The trend towards an elevated basal value in the uninjured leg of the *Shb* knockout is in agreement with the observed increased cremaster flow velocity (Fig. 2). We also concluded that these mice have a sufficient number of collaterals to prevent detectable ischemia in the quadriceps muscle just above the knee. However, exposing the leg to heat revealed significant differences between the wild-type and knockout mice (Fig. 6). The increase in temperature was similar in the wild-type and *Shb* knockout (wild-type 9.4 ± 0.3; *Shb* knockout 8.8 ± 0.2). Whereas blood flow in response to heat was the same in the healthy legs, *Shb* knockout mice subjected to femoral artery occlusion displayed a significantly reduced heat-induced hyperemic response on day 1 and 7 and a trend to a reduction on day 3. Thus this in vivo model of temperature changes after femoral artery ligation confirms the notion that *Shb* deficiency will confer a functional disadvantage to a vascular response. This may be the combined result of structural (arteriolar and capillary) and reactive (angiogenesis and vascular permeability) abnormalities.

Discussion

To therapeutically target the pathological vasculature present in disease, knowledge expansion on physiological function is required. The current study addresses the role of *Shb* in blood vessel formation and function during homeostasis as well as when the vascular system is stressed. For this reason, our current study is an important expansion of our previous work [23]. In our previous study we described aberrant angiogenesis and microvascular endothelium with focus on tumor angiogenesis. In adult muscle under steady state we presently observe alterations of arteriolar supply with increased density of arterioles of a diameter of 48–96 μm and reduced microvascular branchpoints. Blood flow is regulated to a large extent by factors that cause constriction/dilatation of arterioles [8], but the arteriolar alterations that we observe are structural since they are imaged after fixation of the vascular system. The reasons for these changes are unclear and as a whole the formation of the arteriolar system is relatively unexplored. *Shb* could participate directly in this process but alternatively these structural changes may ensue as a consequence of adaptation to

microvascular defects that the absence of *Shb* imposes. Nevertheless, Poiseuille's law predicts altered blood flow as a consequence of these changes since flow depends on vessel diameter. Indeed, we noted an increased flow velocity in the post-arterial cremaster vasculature. The reduced number of microvascular branchpoints and increased vessel length (tortuosity) in the cremaster muscle are most likely a long-term consequence of decreased angiogenesis: this can be inferred from similar findings recorded in Matrigel™ plugs, a system in which active angiogenesis was provoked. Whereas the total vascular density was reduced in the active angiogenesis situation this parameter was not significantly affected in the cremaster vasculature, which indicates that angiogenesis occurs at a slower rate in *Shb* deficient mice but is normalized with time. Since a complete and not an endothelium-specific *Shb* knockout was used the findings raise the possibility that non-endothelial cells participate in the observed responses.

Aberrant staining of VE-cadherin is demonstrated in *Shb* knockout endothelial cells implicating abnormalities in adherens junctions. This staining pattern bears a resemblance to that observed in cortactin deficient mice [28]. Cortactin regulates actin remodeling but it remains uncertain whether that aspect of cortactin function is responsible for the effect on endothelial junctions. Adherens junctions are thought to be of importance for regulation of vascular permeability and conditions that cause increased vascular permeability often alter structural features of junctions [17]. A key player in regulation of these events is the cell adhesion protein VE-cadherin [18] and VEGF-A is thought to via its receptor VEGFR-2 affect the localization and functional characteristics of VE-cadherin [16]. The underlying mechanisms are poorly understood but VEG-FR-2 and VE-cadherin are known to associate with each other [18]. Activation of VEGFR-2 causes Src-dependent VE-cadherin phosphorylation, which may contribute to dissociation of junctions [16, 29]. A parallel pathway involves Rac-activation and serine-phosphorylation of VE-cadherin and presumably dissociation from VEGFR-2 in junctions [30]. A third mechanism depends on the phos-photyrosine-phosphatase VE-PTP that also associates with VEGFR-2 and VE-cadherin [31, 32]. Both VE-cadherin and VEGFR-2 have been shown to internalize upon VEGF-A stimulation and dissociation from adherens junctions [30, 33]. Whereas VEGFR-2 recycles to a large extent to the cell surface [34] the fate of VE-cadherin is less well described. Our in vivo data in cremaster venules suggest that VE-cadherin dissociates from junctions to other cellular compartments in response to VEGF. A similar kind of in vivo dissociation of VE-cadherin from venule junctions in response to VEGF-A has previously been described [35]. As visualized by SEM, this has consequences for the structural features of junctions. Such an effect could not be observed in *Shb* knockout venules. The molecular mechanism behind this response remains unresolved but presumably involves altered VEGFR-2 signaling. *Shb* is a multi-domain adapter protein that may interact with Src kinases, PLCγ, PI3kinase, FAK, Crk and ras-GAP [36], and consequently, perturbations in one or several of these signaling pathways may yield the presently observed results. Thus, one potential signaling intermediate of interest is c-Src and it would be intriguing to know if a c-Src inhibitor like Tris (Dibenzylideneacetone) Dipalladium [37] would phenocopy the *Shb* knockout phenotype with respect to altered vascular permeability. Nevertheless, *Shb* deficiency will have consequences for the structure of adherens junctions and their function. This is most clearly demonstrated by the altered physiological response to cremaster arterial

ligation, in which the vascular permeability was reduced 24 h after the procedure. Vascular ligation causes local ischemia with VEGF production and increased vascular permeability as a consequence. Apparently this response fails in the *Shb* knockout, which could impair the healing process.

A reduced blood flow response to warming of the leg in *Shb* knockout mice was also noted after femoral artery occlusion. This further reinforces the notion that *Shb* deficiency indeed has negative consequences for the vasculature that can be compensated for under steady-state but confer insufficiency when the vasculature is stressed. This deficiency may be the consequence of both reduced vascular permeability and compensatory angiogenesis.

In conclusion, *Shb* deficiency affected the vascular structure under steady state, the angiogenic and the vascular permeability responses under vascular stress and consequently *Shb* plays an important role in vascular homeostasis.

Supplementary Material

Refer to Web version on PubMed Central for supplementary material.

Acknowledgments

We are grateful to Marianne Ljungkvist for help with SEM and Ying Gou for help with blood flow measurements. The work was supported by the Swedish Cancer Foundation (100494), the Swedish Research Council (K2011-54X-10822), the Swedish Diabetes Fund and Family Ernfors Fund.

References

1. Folkman J, Watson K, Ingber D, Hanahan D. Induction of angiogenesis during the transition from hyperplasia to neoplasia. Nature. 1989; 339(6219):58–61.10.1038/339058a0 [PubMed: 2469964]
2. Weis SM. Vascular permeability in cardiovascular disease and cancer. Curr Opin Hematol. 2008; 15(3):243–249.10.1097/MOH.0b013e3282f97d86 [PubMed: 18391792]
3. Olsson AK, Dimberg A, Kreuger J, Claesson-Welsh L. VEGF receptor signalling—in control of vascular function. Nat Rev Mol Cell Biol. 2006; 7(5):359–371.10.1038/nrm1911 [PubMed: 16633338]
4. Matsumoto T, Claesson-Welsh L. VEGF receptor signal transduction. Sci STKE. 2001; 2001(112):re21.10.1126/stke.2001.112.re21 [PubMed: 11741095]
5. Praidou A, Androudi S, Brazitikos P, Karakiulakis G, Papakonstantinou E, Dimitrakos S. Angiogenic growth factors and their inhibitors in diabetic retinopathy. Curr Diabetes Rev. 2010; 6(5):304–312. [PubMed: 20594164]
6. Bhadada SV, Goyal BR, Patel MM. Angiogenic targets for potential disorders. Fundam Clin Pharmacol. 2011; 25(1):29–47.10.1111/j.1472-8206.2010.00814.x [PubMed: 20199582]
7. Murakami M, Simons M. Fibroblast growth factor regulation of neovascularization. Curr Opin Hematol. 2008; 15(3):215–220.10.1097/MOH.0b013e3282f97d98 [PubMed: 18391788]
8. Casey DP, Joyner MJ. Local control of skeletal muscle blood flow during exercise: influence of available oxygen. J Appl Physiol. 201110.1152/japplphysiol.00895.2011
9. Burnstock G. Physiology and pathophysiology of purinergic neurotransmission. Physiol Rev. 2007; 87(2):659–797.10.1152/physrev.00043.2006 [PubMed: 17429044]
10. Liu D, Krueger J, Le Noble F. The role of blood flow and microRNAs in blood vessel development. Int J Dev Biol. 2011; 55(4–5):419–429.10.1387/ijdb.103220dl [PubMed: 21858767]
11. Swift MR, Weinstein BM. Arterial-venous specification during development. Circ Res. 2009; 104(5):576–588.10.1161/CIRCRESAHA.108.188805 [PubMed: 19286613]

12. Lanahan AA, Hermans K, Claes F, Kerley-Hamilton JS, Zhuang ZW, Giordano FJ, Carmeliet P, Simons M. VEGF receptor 2 endocytic trafficking regulates arterial morphogenesis. Dev Cell. 2010; 18(5):713–724.10.1016/j.devcel.2010.02.016 [PubMed: 20434959]

13. Rolny C, Mazzone M, Tugues S, Laoui D, Johansson I, Coulon C, Squadrito ML, Segura I, Li X, Knevels E, Costa S, Vinckier S, Dresselaer T, Akerud P, De Mol M, Salomaki H, Phillipson M, Wyns S, Larsson E, Buysschaert I, Botling J, Himmelreich U, Van Ginderachter JA, De Palma M, Dewerchin M, Claesson-Welsh L, Carmeliet P. HRG inhibits tumor growth and metastasis by inducing macrophage polarization and vessel normalization through downregulation of PlGF. Cancer Cell. 2011; 19(1):31–44.10.1016/j.ccr.2010.11.009 [PubMed: 21215706]

14. Carmeliet P, Jain RK. Principles and mechanisms of vessel normalization for cancer and other angiogenic diseases. Nat Rev Drug Discov. 2011; 10(6):417–427.10.1038/nrd3455 [PubMed: 21629292]

15. Ferrara N. Vascular endothelial growth factor: basic science and clinical progress. Endocr Rev. 2004; 25(4):581–611.10.1210/er.2003-002725/4/581 [PubMed: 15294883]

16. Weis S, Shintani S, Weber A, Kirchmair R, Wood M, Cravens A, McSharry H, Iwakura A, Yoon YS, Himes N, Burstein D, Doukas J, Soll R, Losordo D, Cheresh D. Src blockade stabilizes a Flk/cadherin complex, reducing edema and tissue injury following myocardial infarction. J Clin Invest. 2004; 113(6):885–894.10.1172/JCI20702 [PubMed: 15067321]

17. Dejana E, Tournier-Lasserve E, Weinstein BM. The control of vascular integrity by endothelial cell junctions: molecular basis and pathological implications. Dev Cell. 2009; 16(2):209–221.10.1016/j.devcel.2009.01.004 [PubMed: 19217423]

18. Carmeliet P, Lampugnani MG, Moons L, Breviario F, Compernolle V, Bono F, Balconi G, Spagnuolo R, Oosthuyse B, Dewerchin M, Zanetti A, Angellilo A, Mattot V, Nuyens D, Lutgens E, Clotman F, de Ruiter MC, Gittenberger-de Groot A, Poelmann R, Lupu F, Herbert JM, Collen D, Dejana E. Targeted deficiency or cytosolic truncation of the VE-cadherin gene in mice impairs VEGF-mediated endothelial survival and angiogenesis. Cell. 1999; 98(2):147–157. [PubMed: 10428027]

19. Dvorak HF. Angiogenesis: update 2005. J Thromb Haemost. 2005; 3(8):1835–1842.10.1111/j.1538-7836.2005.01361.x [PubMed: 16102050]

20. Baluk P, Hirata A, Thurston G, Fujiwara T, Neal CR, Michel CC, McDonald DM. Endothelial gaps: time course of formation and closure in inflamed venules of rats. Am J Physiol. 1997; 272(1 Pt 1):L155–L170. [PubMed: 9038915]

21. Baffert F, Le T, Thurston G, McDonald DM. Angiopoietin-1 decreases plasma leakage by reducing number and size of endothelial gaps in venules. Am J Physiol Heart Circ Physiol. 2006; 290(1):H107–H118.10.1152/ajpheart.00542.2005 [PubMed: 16126815]

22. Holmqvist K, Cross MJ, Rolny C, Hagerkvist R, Rahimi N, Matsumoto T, Claesson-Welsh L, Welsh M. The adaptor protein shb binds to tyrosine 1175 in vascular endothelial growth factor (VEGF) receptor-2 and regulates VEGF-dependent cellular migration. J Biol Chem. 2004; 279(21):22267–22275.10.1074/jbc.M312729200M312729200 [PubMed: 15026417]

23. Funa NS, Kriz V, Zang G, Calounova G, Akerblom B, Mares J, Larsson E, Sun Y, Betsholtz C, Welsh M. Dysfunctional microvasculature as a consequence of shb gene inactivation causes impaired tumor growth. Cancer Res. 2009; 69(5):2141–2148.10.1158/0008-5472.CAN-08-3797 [PubMed: 19223532]

24. Kriz V, Mares J, Wentzel P, Funa NS, Calounova G, Zhang XQ, Forsberg-Nilsson K, Forsberg M, Welsh M. Shb null allele is inherited with a transmission ratio distortion and causes reduced viability in utero. Dev Dyn. 2007; 236(9):2485–2492.10.1002/dvdy.21257 [PubMed: 17676633]

25. Zagorchev L, Oses P, Zhuang ZW, Moodie K, Mulligan-Kehoe MJ, Simons M, Couffinhal T. Micro computed tomography for vascular exploration. J Angiogenes Res. 2010; 2:7.10.1186/2040-2384-2-7 [PubMed: 20298533]

26. Zhuang ZW, Gao L, Murakami M, Pearlman JD, Sackett TJ, Simons M, de Muinck ED. Arteriogenesis: noninvasive quantification with multi-detector row CT angiography and three-dimensional volume rendering in rodents. Radiology. 2006; 240(3):698–707.10.1148/radiol.2403050976 [PubMed: 16926325]

27. Limbourg A, Korff T, Napp LC, Schaper W, Drexler H, Limbourg FP. Evaluation of postnatal arteriogenesis and angiogenesis in a mouse model of hind-limb ischemia. Nat Protoc. 2009; 4(12): 1737–1746.10.1038/nprot.2009.185 [PubMed: 19893509]
28. Schnoor M, Lai FP, Zarbock A, Klaver R, Polaschegg C, Schulte D, Weich HA, Oelkers JM, Rottner K, Vestweber D. Cortactin deficiency is associated with reduced neutrophil recruitment but increased vascular permeability in vivo. J Exp Med. 2011; 208(8):1721–1735.10.1084/jem.20101920 [PubMed: 21788407]
29. Eliceiri BP, Paul R, Schwartzberg PL, Hood JD, Leng J, Cheresh DA. Selective requirement for Src kinases during VEGF-induced angiogenesis and vascular permeability. Mol Cell. 1999; 4(6): 915–924. [PubMed: 10635317]
30. Gavard J, Gutkind JS. VEGF controls endothelial-cell permeability by promoting the beta-arrestin-dependent endocytosis of VE-cadherin. Nat Cell Biol. 2006; 8(11):1223–1234.10.1038/ncb1486 [PubMed: 17060906]
31. Mellberg S, Dimberg A, Bahram F, Hayashi M, Rennel E, Ameur A, Westholm JO, Larsson E, Lindahl P, Cross MJ, Claesson-Welsh L. Transcriptional profiling reveals a critical role for tyrosine phosphatase VE-PTP in regulation of VEGFR2 activity and endothelial cell morphogenesis. Faseb J. 2009; 23(5):1490–1502.10.1096/fj.08-123810 [PubMed: 19136612]
32. Nottebaum AF, Cagna G, Winderlich M, Gamp AC, Linnepe R, Polaschegg C, Filippova K, Lyck R, Engelhardt B, Kamenyeva O, Bixel MG, Butz S, Vestweber D. VE-PTP maintains the endothelial barrier via plakoglobin and becomes dissociated from VE-cadherin by leukocytes and by VEGF. J Exp Med. 2008; 205(12):2929–2945.10.1084/jem.20080406 [PubMed: 19015309]
33. Lampugnani MG, Orsenigo F, Gagliani MC, Tacchetti C, Dejana E. Vascular endothelial cadherin controls VEGFR-2 internalization and signaling from intracellular compartments. J Cell Biol. 2006; 174(4):593–604.10.1083/jcb.200602080 [PubMed: 16893970]
34. Gampel A, Moss L, Jones MC, Brunton V, Norman JC, Mellor H. VEGF regulates the mobilization of VEGFR2/KDR from an intracellular endothelial storage compartment. Blood. 2006; 108(8):2624–2631.10.1182/blood-2005-12-007484 [PubMed: 16638931]
35. Cai J, Wu L, Qi X, Shaw L, Li Calzi S, Caballero S, Jiang WG, Vinores SA, Antonetti D, Ahmed A, Grant MB, Boulton ME. Placenta growth factor-1 exerts time-dependent stabilization of adherens junctions following VEGF-induced vascular permeability. PLoS ONE. 2011; 6(3):e18076.10.1371/journal.pone.0018076 [PubMed: 21464949]
36. Anneren C, Lindholm CK, Kriz V, Welsh M. The FRK/RAK-SHB signaling cascade: a versatile signal-transduction pathway that regulates cell survival, differentiation and proliferation. Curr Mol Med. 2003; 3(4):313–324. [PubMed: 12776987]
37. Bhandarkar SS, Bromberg J, Carrillo C, Selvakumar P, Sharma RK, Perry BN, Govindarajan B, Fried L, Sohn A, Reddy K, Arbiser JL. Tris (dibenzylideneacetone) dipalladium, a N-myristoyltransferase-1 inhibitor, is effective against melanoma growth in vitro and in vivo. Clin Cancer Res. 2008; 14(18):5743–5748.10.1158/1078-0432.CCR-08-0405 [PubMed: 18794083]

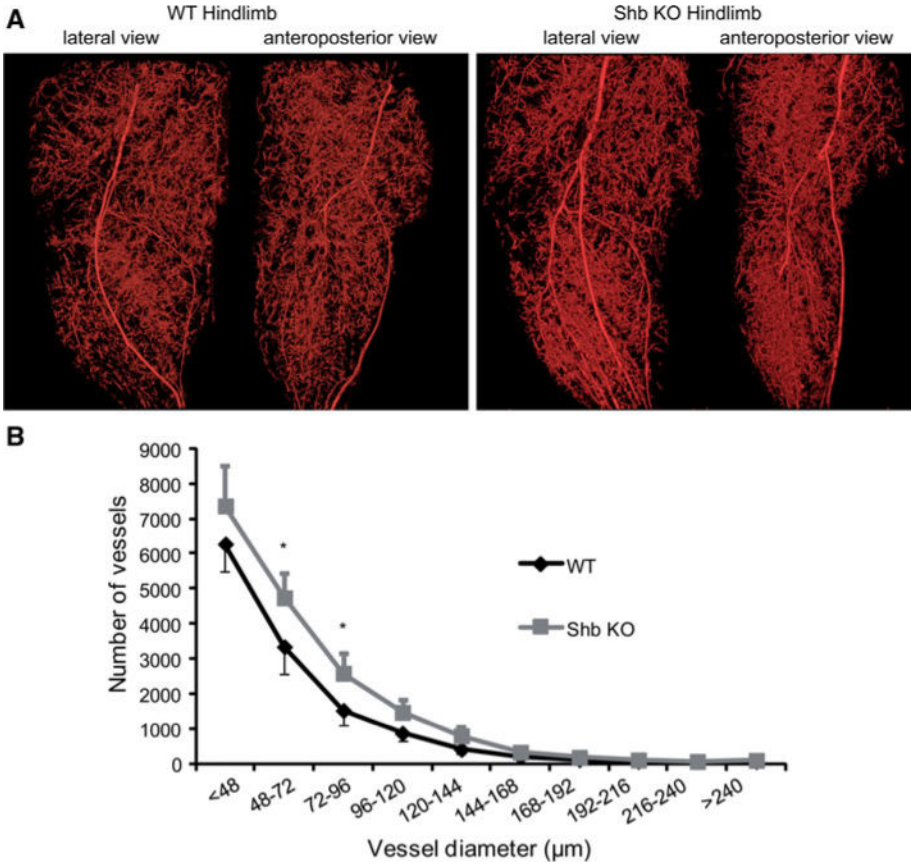

Fig. 1.

Micro-CT analysis of hind-limb arteries in wild-type and *Shb* knockout mice. The figure shows the visualization of arterial tree (**a**) and quantitation of the calf vasculature (**b**). The number of vessels in the different size ranges are shown. Means ± SEM are given. $p < 0.05$ when comparing the wild-type and *Shb* knockout vessel numbers. n = 6 mice for each genotype

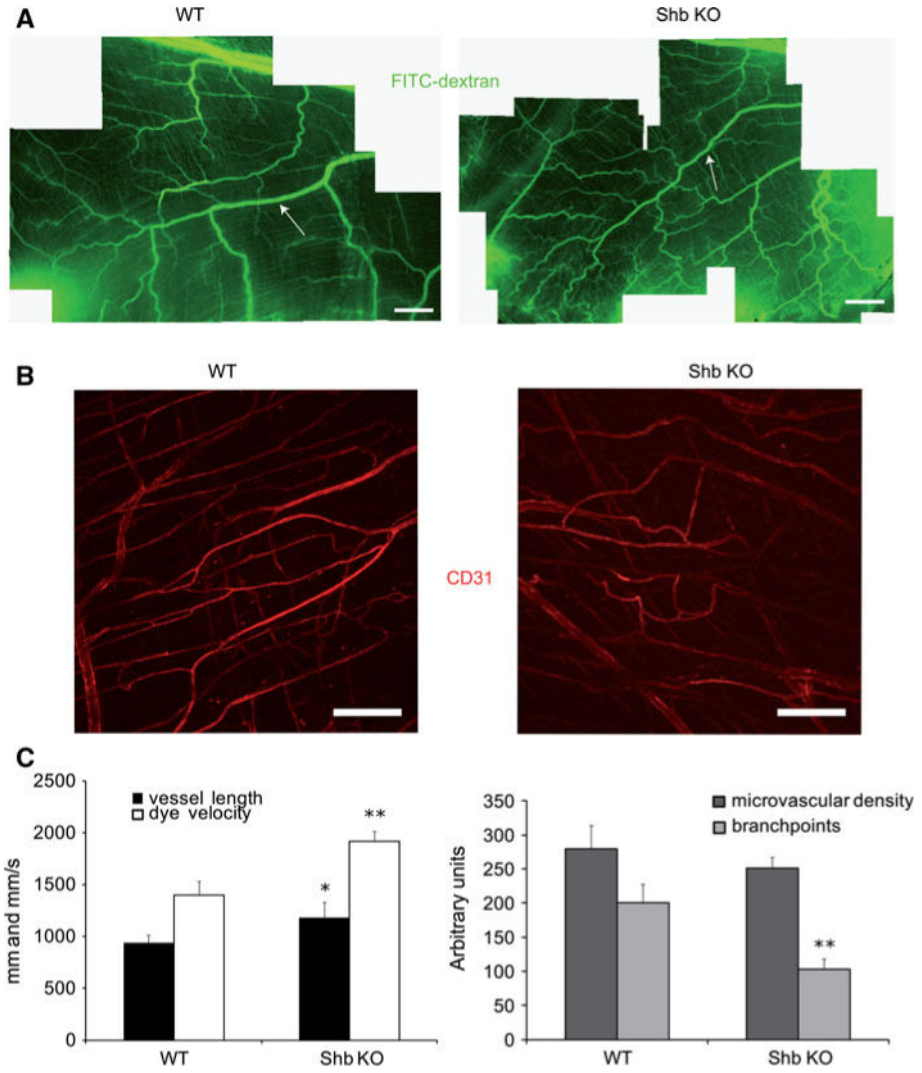

Fig. 2.

Analysis of cremaster vasculature in wild-type and *Shb* knockout mice. **a** Panoramic overviews of cremaster vasculature showing primarily arteries/arterioles after FITC-dextran injection. Scale bar 100 μm. Microscope used was DM5000B, ×5/0.12 or ×10/0.25 objectives (Leica Microsystems, Germany). **b** Whole-mount staining of cremaster microvasculature for CD31 to visualize smaller vessels. Scale bar 200 μm. Microscope used was a laser scanning confocal miscroscope C-1 with Plan Fluor ELWD ×20/0.45 and ×40/0.60 objectives; EZ-C1 software, (Nikon, Japan). (C) Quantitation of vessel length (μm) from a larger artery (A shows examples at top in the panels) to a corresponding vein and dye velocity (mm/s) are given as means ± SEM. * and ** indicate $p < 0.05$ and 0.01, respectively when compared with corresponding wild-type controls using a Students' *t* test. N = 13–16 observations on three mice of each genotype. Quantitation of microvascular density and branchpoints. Values are in arbitrary units as means ± SEM for n = 5–7 observations on 3 mice of each genotype. ** indicates $p < 0.01$ when compared against wild-type with a Students' *t* test

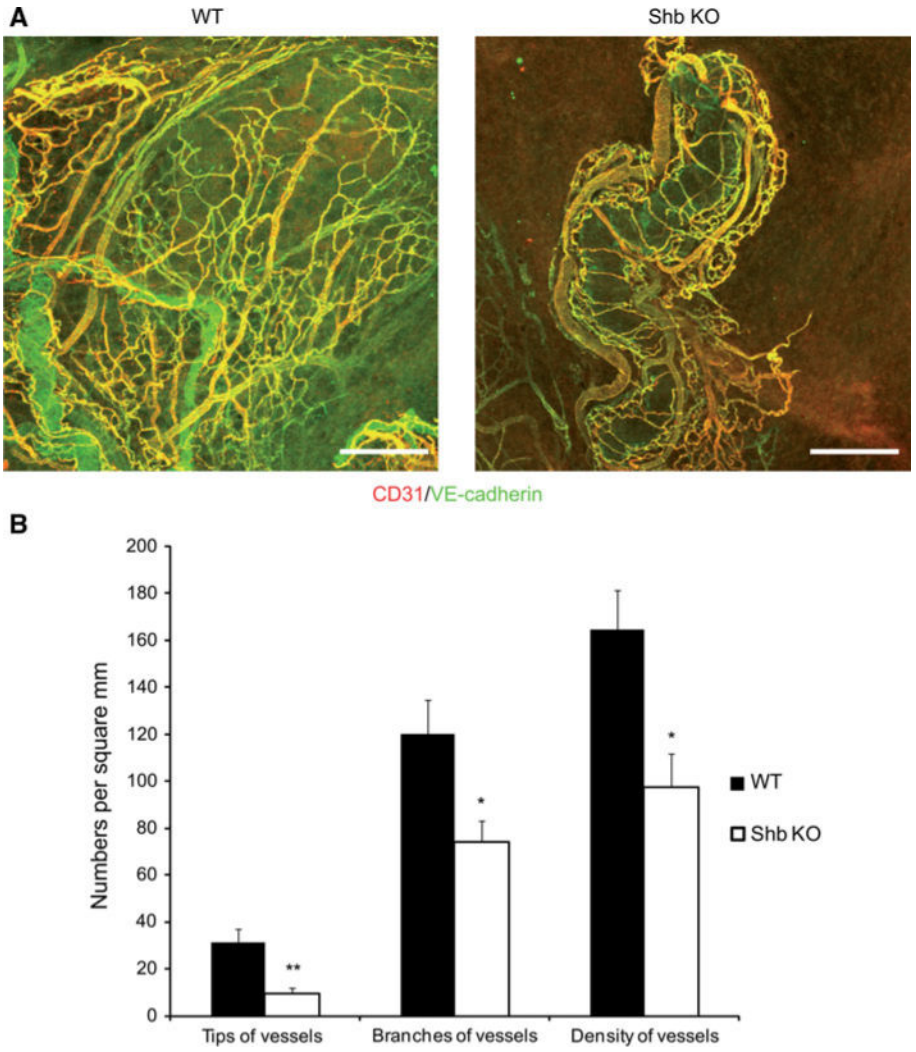

Fig. 3.

Matrigel™ angiogenesis in wild-type and *Shb* knockout mice. **a** The vasculature was stained with CD31 (*red*) and VE-cadherin (*green*) and angiogenesis was estimated by confocal microscopy of zeta-stacks. Scale bar 50 μm. **b** Quantification of angiogenesis by counting vessel tips, vessel branches and vessel density. Values (counts per mm^2) are means ± SEM, n = 3 mice each genotype. * and ** indicate $p < 0.05$ and 0.01, respectively, when compared with wild-type by Students' *t* test

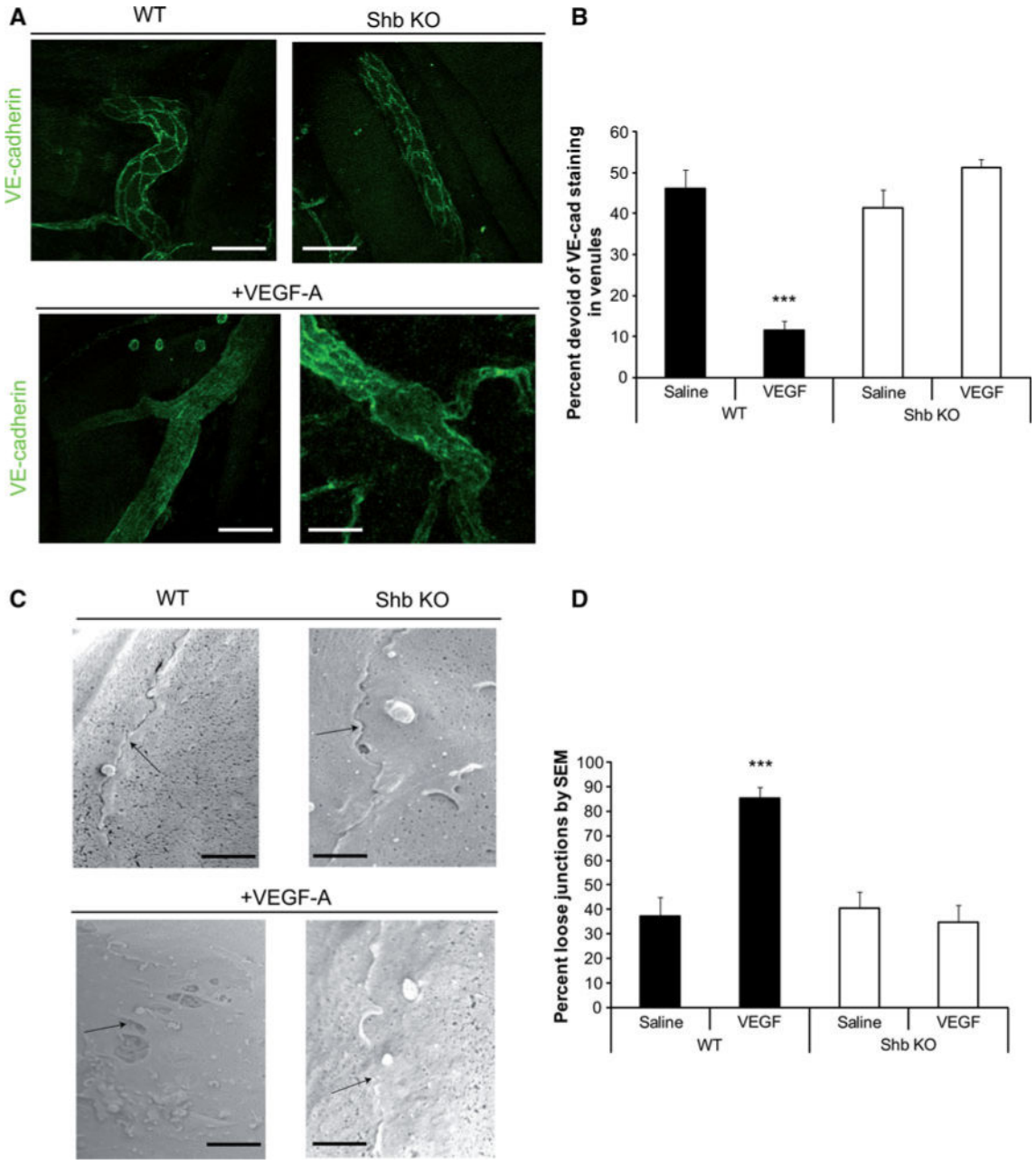

Fig. 4.

Staining of wild-type and *Shb* knockout venules with VE-cadherin (**a, b**) and their ultrastructure visualized by scanning electron microscopy (SEM) (**c, d**). **a** Confocal microscopy of cremaster venules with or without treatment with VEGF-A after staining for VE-cadherin. Cremaster vasculature was injected with 20 ng/ml VEGF-A or PBS and fixated 5 min later. Microscope used was a laser scanning confocal miscroscope C-1 with Plan Fluor ELWD ×40/0.60 and ×60/1.40 objectives; EZ-C1 software, (Nikon, Japan). Original magnification 9400. Scale bars 30 μm. **b** Quantitation of the relative venular surface devoid of VE-cadherin staining in percent. Means ± SEM for 3–5 observations on 3 mice in each genotype are given. *** indicates $p < 0.001$ when compared with unstimulated

wild-type. **c** The muscles had been exposed for 5 min to 20 ng/ml VEGF-A or not. *Arrows* indicate examples of junctions. A LEO 1530 instrument was used. Magnification ×60,000. *Arrows* indicate examples of closed junctions (unstimulated wild-type, VEGF-A stimulated *Shb* knockout), loose junctions (unstimulated *Shb* knockout) and porous junctions (VEGF-A stimulated wild-type). *Scale bar* 1 μm. **d** Quantitation of the percentages loose or porous adherens junctions in the corresponding groups for 6–12 determinations on 3 mice in each genotype. *** indicates $p < 0.001$ when compared with unstimulated wild-type

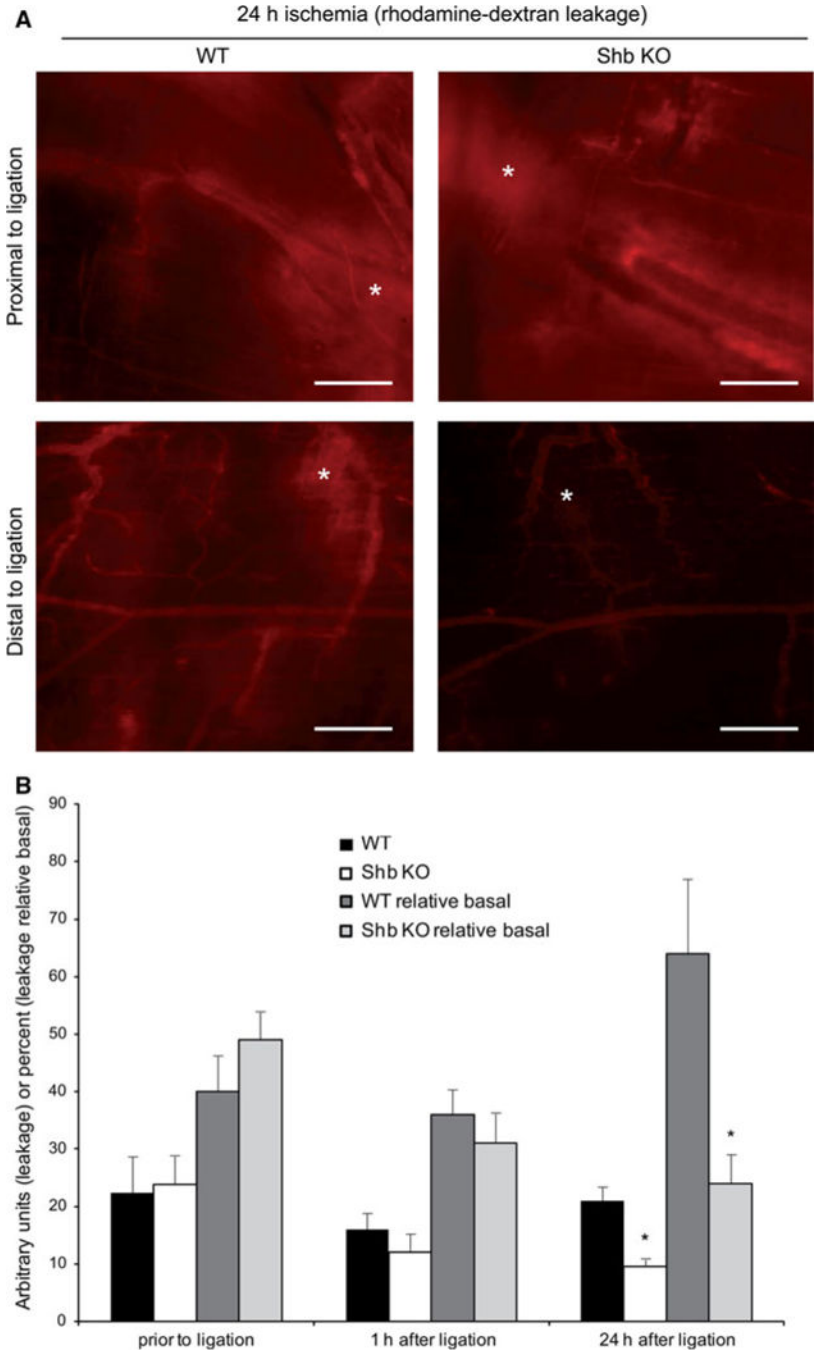

Fig. 5.

Vascular leakage in response to arterial ligation in wild-type or *Shb* knockout cremaster muscles. **a** Rhodamine-dextran leakage at 24 h after ischemia at sites proximal and distal to the site of ligation. Scale bar 100 μm. Microscope used was DM5000B, ×5/0.12 or ×10/ 0.25 objectives (Leica Microsystems, Germany). **b** Rhodamine-dextran fluorescence was determined in several microscopic fields proximal or distal to the site of ligation prior to ligation, 1 h after ligation and 24 h after ligation. Values are absolute fluorescence distal to ligation or fluorescence distal to ligation relative the corresponding value proximal to

ligation (basal). Means ± SEM for 3–5 mice of each genotype at each point are given. * indicates $p < 0.05$ when compared with control using a Students' *t* test. *Asterisks* show examples of extravascular leakage of the fluorescent dye. Note differences in signal

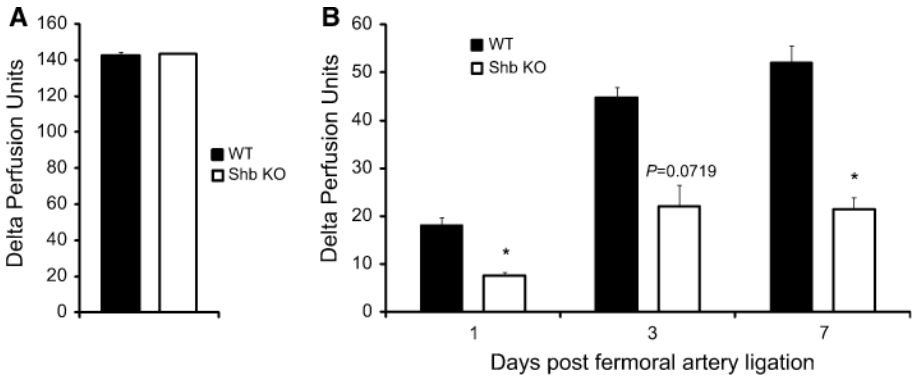

Fig. 6.

Analysis of blood flow changes in response to heat in wild-type and *Shb* knockout mice subjected to unilateral femoral artery ligation. Perfusion changes in response to heat (30 °C) in contralateral non-occluded (**a**) and occluded (**b**) wild-type and *Shb* knockout mice. Limb perfusion changes in response to heat challenge were measured on day 1, 3 and 7 after arterial occlusion after base line registration. Data from the contralateral non-occluded leg were compiled (**a**). Values are expressed as delta perfusion units and means ± SEM are given. n = 5 mice for each genotype. * indicates $p < 0.05$ when compared with corresponding wild-type control